ELSEVIER

Journal of Nuclear Materials 266–269 (1999) 240–246

journal of nuclear materials

Deposition of a-C/B:D layers by ICRF-wall conditioning in TEXTOR-94

H.G. Esser [a,*], A.I. Lyssoivan [b,1], M. Freisinger [b,1], P. Karduck [c], R. Koch [b,1], V. Philipps [a], H. Reimer [a], M. Rubel [d], J. von Seggern [a], M. Vervier [b,1], P. Wienhold [a]

[a] *Institut für Plasmaphysik, Forschungszentrum Jülich GmbH, EURATOM Association, D-52425 Jülich, Germany*
[b] *Laboratoire de Physique des Plasmas/Laboratorium voor Plasmaphysica, ERM/KMS, EURATOM Association, B-1000, Brussels, Belgium*
[c] *Central Facility for Electron Microscopy, Aachen University of Technology, D-52056 Aachen, Germany*
[d] *Alfven Laboratory, Royal Institute of Technology, Association EURATOM-NFR, Teknikringen 31, 10044 Stockholm, Sweden*

Abstract

Wall conditioning and especially wall coating procedures like boronization or siliconization are indispensable for present day machines. They are also needed for future steady state plasma devices with superconducting coils and permanent magnetic fields like ITER. However, since important standard conditioning techniques like Plasma Chemical Vapor Deposition (PCVD), based on dc-glow discharges, are not compatible with those fields, new techniques have to be developed. This paper reports on first ion cyclotron range of frequency (ICRF)-assisted in situ deposition of a boron and carbon containing layer of relevant thickness onto the first wall of a tokamak. The new method is called ion cyclotron coating (ICC) and is based on ICRF plasma production in gas mixtures containing appropriate reactive precursor molecules. The new method is compatible with the magnetic field since it depends on its presence in order to produce a plasma. The geometrical arrangement of necessary facilities and their characteristic parameters for ICC in TEXTOR-94 will be described as well as the experimental procedure. The ICC-process itself and the properties of the produced layer will be presented.

Keywords: Wall conditioning; Wall coating; C(B):H film; TEXTOR; ICRF; Impurity reduction; Boronized carbon film; Film growth rate; First wall; Plasma performance

1. Introduction and motivation

Wall conditioning in general is well accepted as a must for future fusion devices like ITER. It is indispensable after openings, major leaks or other abnormal events. The conditioning status of the wall will play also a key role to obtain appropriate plasma confinement scenarios like H-mode or RI-mode [1]. In present day machines wall treatment by plasma chemical vapor deposition (PCVD), based on dc-glow discharges, is the common and frequently used conditioning techniques. Plasma parameters like density, dilution, recycling, radiation, isotope ratio etc can be controlled or at least influenced, leading to a general improvement of the plasma performance [2]. Dc-glow discharge will not be applicable in future long pulse machines due to its incompatibility with the steady state toroidal magnetic fields. New techniques have to be developed to make wall conditioning possible also in the future. Recent studies of ion cyclotron range of frequency (ICRF) wall conditioning in TEXTOR-94 [3] and in Tore Supra [4] reveal this technique to become more and more a reliable alternative conditioning method. In addition a lot of experience concerning ICRF plasma production in TEXTOR-94 was gained aiming on the improvement of

* Corresponding author. Tel.: +49 2461 61 5620; fax: +49 2461 61 2660; e-mail: h.g.esser@fz-juelich.de
[1] Partner in the Trilateral Euregio Cluster.

0022-3115/99/$ – see front matter
PII: S0022-3115(98)00576-5

start-up scenarios in TEXTOR-94 [5]. Work on the field of ICRF wall conditioning focused up to now more on the study of plasma production and its characterization. The attention concerning its application was mostly turned to hydrogen desorption from the first wall, using helium and wall cleaning using deuterium [3,6] as working gases.

This paper reports on recent results obtained in TEXTOR-94 concerning ion cyclotron coating (ICC). The suitability of the new technique will be shown, to apply proven wall coating concepts like carbonization [7] boronization [8] or siliconization [9]. The results from various surface analyses methods will be presented and the deposited layer will be characterized.

2. Experimental

The aim of the experiment was to demonstrate, that an rf-plasma, produced by an ICRF-system, is a suitable in situ technique for wall coating of fusion devices. Due to safety requirements [10] deuterated trimethyl-boron $B(CD_3)_3$ (TMB), was selected for this experiment as an appropriate reactive precursor gas. It is less hazardous than Diborane [11], which is the regular gas for standard boronizations in TEXTOR-94. The TMB was mixed with helium. This mixture has been used earlier successfully in TEXTOR-94 as fueling gas for conditioning in running discharges [12].

2.1. Experimental set up and conditions

TEXTOR-94 is divided toroidally into 16 regular sectors by the magnetic field coils which also define the names of the sectors (Fig. 1). The direction of the toroidal magnetic field B_t ($0 \leqslant B_t$ [T] $\leqslant 2.6$) is defined as positive with increasing coil numbers. The duration of B_t depends on the field strength and is limited by ohmic heating of the coils. It varies from a steady state operation mode for $B_t \leqslant 0.4$ [T] to a pulsed mode operation mode with a duty cycle of 8 s flat top every 5 min for $B_t = 2.6$ T. The first wall of TEXTOR-94, has an area of about 38 m^2 and consists mainly of a 1 mm thick heatable toroidal Inconel 625 liner ($RT \leqslant T_l$ [K] $\leqslant 620$) with a major radius R of 175 cm and a minor one r_a of 55 cm. The fraction of the area of the holes in the liner for diagnostic purposes is of the order of 15%. Obstacles, like ICRF-antennas, small protection limiters at different places, 8 ALT II limiter blades (3.5 m^2) and the inner bumper limiter (6 m^2) cover the inner wall of the liner to a large extent. They consist of fine grain graphite and are positioned radially between $46 \leqslant r_a$ [cm] $\leqslant 55$ cm. The orientation of these surfaces with respect to the magnetic field varies from parallel to perpendicular.

The working gas consists of helium and TMB. It was mixed by two independent feed back controlled gas lines.

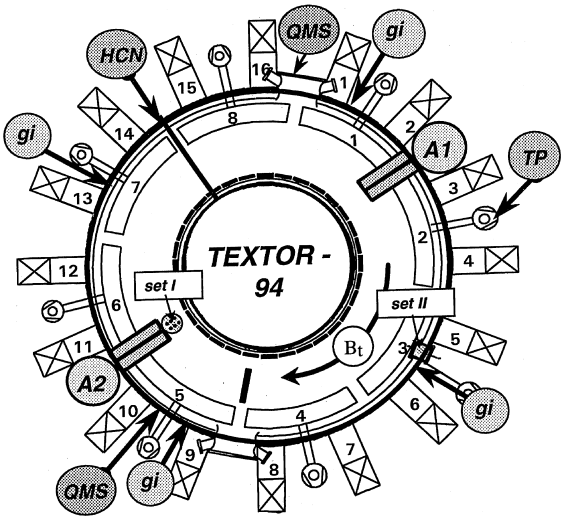

Fig. 1. Top view of TEXTOR-94; arrangement of ICC-facilities.

This gives high flexibility with respect to total gas pressure as well as gas ratio in the vessel. The gas mixture was distributed around the torus and evenly filled into the vacuum vessel at four gas inlet ports (gi) in the sectors 1/2, 5/6, 9/10 and 13/14. To establish the appropriate gas pressure and through flow of the gas, TEXTOR was pumped by the eight turbo molecular pumps (TP) which are distributed around the torus beneath the eight ALT-II limiter blades. The average of the pumping speed is about $S_{eff,\,He} = 320$ l/s for each TP in the molecular flow range. All pump exhausts were equipped with thermal decomposers between TPs and roots blowers, heatable to above 970 K to decompose reactive gases. This ensures, beside other preventive steps, the appropriate handling and disposal of the toxic and explosive gas TMB according to the rules. In addition filters extracting fine grain powder were installed in each line, to protect the roots blowers and fore pumps. These steps concerning safety requirements reduced the vacuum conductance by nearly a factor of 2. Calibrated dynamic measurements of gas pressures and partial pressures in the vacuum vessel provide the quantitative determination of the gas amounts and species entering and leaving the vessel for particle balance. To prevent the destruction of the ionization gauges by the reactive gas TMB, all systems were switched off and the total pressure was measured by capacitive manometers (CM) (baratron). Quadrupol mass spectrometers (QMS) were used to measure the partial pressure in sectors 9/10 and 16/1.

Rf-plasmas have been produced under various conditions in TEXTOR using the existing ICRF-system designed for plasma heating experiments. This comprises two double-loop antennas, (A1) shielded and (A2) unshielded [13]. The antennas are positioned at the low

magnetic field side at locations toroidally opposite. A1 in sector 2/3, A2 in sector 10/11, see Fig. 1. The current straps in the antennas were fed either out phase or in phase. The power can be applied to both antennas from separate rf-generators in the frequency range of $25 \leqslant f_{g,i}$ (MHz)<38 and in the power range of $P_{RFi}<2$ MW; with $f_{g,i}$ = the generator frequency and P_{RFi} = the rf-power for the two antennas $i=1$ and $i=2$ in overlapping or sequential pulses. Pulsed operation mode of the antennas was usually used for ICRF-wall conditioning experiments. The antennas structures are not actively cooled. This limits the duration of steady state plasma production depending on power. Like for ECRH, the ICRF-discharges are produced by the absorption of rf-energy by electrons in the presence of a toroidal magnetic field B_t. The rf-electric field $\tilde{E}\|$parallel to the B_t field is believed to be responsible for neutral gas breakdown and plasma build-up. It obviously satisfies the criterion for ionization in TEXTOR-94 [14]. The $\tilde{E}\|$-component may be generated by TEXTOR ICRF poloidal antennas mainly due to the rf-voltage difference between the antenna central conductor and the side protection rf-limiters of the antenna box [15]. After the first phase of neutral gas ionization in the antenna near field, as electron plasma frequency $\omega_{pe} = (4\pi n_e e^2/m_e^3)^{1/2}$ (here n_e is the electron density, e and m_e are the electron charge and mass, respectively) becomes of the order of the operating angular frequency $\omega = 2\pi f_g$ (f_g = generator frequency), plasma waves can start propagating, causing further volume ionization of the neutral gas and plasma buildup in the torus.

Because of the very low plasma temperature during the ionization phase ($T_e \sim 3$–5 eV [14]) the rf-power is expected to be dissipated mostly collisionally. Such a non-resonant coupling of rf-power allows plasma production at any B_t, as confirmed by our experimental observations. Helium plasmas with central line averaged densities up to $\bar{n}_e(0) \sim 6 \times 10^{12}$ cm^{-3} in the best cases were reliably produced in a wide range of toroidal magnetic field ($0.21 \leqslant B_t$ [T] $\leqslant 2.24$) without changing the rf-generator frequency ($f_g = 32.5$ MHz).

The poloidal cross section of the line averaged electron density of the rf-plasma was measured by a 9 channel HCN interferometer in sector 14/15.

2.2. Wall samples, exposure positions and ex situ analyses

An indispensable method to determine the properties of first wall layers is the exposure of wall samples to the deposition process. The subsequent measured layer properties and the methods to obtain them are listed below:

Ellipsometry: absorption constant k, refraction constant n and thickness.

Electron Probe X-ray Microanalysies (*EPMA*): areal mass density of boron, carbon, oxygen.

Sputter Auger: relative mass concentrations of boron, carbon, and oxygen in depth.

Interference Fringe Analysis: thickness mapping from colors.

Nuclear Reaction Analysis (*NRA*): areal mass densities of deuterium, boron, carbon, and oxygen.

Three sample holder plates as shown in Fig. 2 (size 76 mm × 50 mm) (Al and SS) equipped with circular samples (7 mm in diameter); of silicon, graphite, stainless steel and Inconel 625 have been exposed during the experiment at different positions of the liner. The discs and the sample holder were analyzed, the latter one along the line AB as shown in Fig. 2. The pattern across the plate shown in the figure is due to the deposited layer and will be discussed later. One of the plates, made from stainless steel, was placed at the torus bottom in sector 10/11 (Fig. 1) on liner position ($r_a = 55$ cm), which is also the sector of the ICRF antenna A2. This position is defined as sample set I. It was equipped with four silicon specimens, one of stainless steel, one of Inconel 625, and one of graphite (EK98). Sample set II consists of two aluminum plates equipped with specimens in the same way as the plate of set I. It was inserted in the midplane of the torus through a liner hole of 100 mm diameter in sector 5/6. A gap of about 20 mm was between the liner and the plates. The sample reached about 50 mm through the hole into the rf-deposition plasma. One of the plates was aligned with the surface toward the top and the other toward the bottom. All sample surfaces, set I and set II, were oriented parallel to the toroidal magnetic field B_t.

2.3. Ion cyclotron coating (ICC): procedure and parameters

The experiment was carried out in the so called pulsed operation mode i.e. the ICRF-plasma was produced simultaneously by the two antennas for about 200

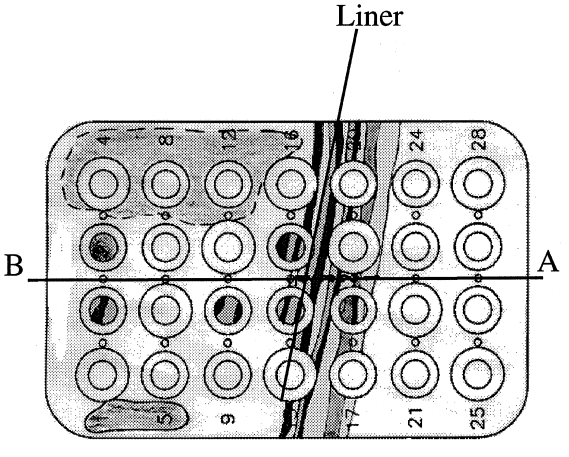

Fig. 2. Plates for wall sample exposures (7.6 cm × 5 cm).

ms followed by a pause of about 3600 ms. The whole process time lasted 120 min. This operation mode prevents the overheating of the antenna and allows the gas mixture to distribute uniformly inside the torus in-between rf-plasma pulses until the molecules are ionized and fixed to the magnetic field lines. The magnetic field was kept constant at a value of $B_t(0) = 0.21$ T on axis during the whole time. The liner was at about 460–480 K. To find appropriate parameter values for the layer deposition, a study of a plasma production as function of total pressure and gas mixture was carried out prior to the experiment. Plasma production was easily achieved in the concentration range of $5 \leqslant C_{TMB}$ [%] $\leqslant 61$. The parameters for the ion cyclotron coating process (ICC) are listed in Table 1.

The natural leak rate of TEXTOR-94 during the experiment was 8×10^{-5} mbar l/s. The temperature of the samples was transient and estimated to be 300 K at the beginning, heated to 390 K at the end, due to radiation from the liner.

3. Results and discussion

3.1. Characterization of the ICRF plasma

Reliable and reproducible plasma production was obtained for the nearly 2000 plasma pulses. Both ICRF antennas worked constantly well during the layer deposition experiment. Antenna 1, with Faraday screen, positioned in sector 2/3, coupled 150 kW with an efficiency $\eta_1 = 81\%$ and antenna 2, in sector 10/11, without Faraday screen, 170 kW with $\eta_2 = 91\%$ to the rf-plasma volume of about 10.5 m^3. This leads to a power density of about 30 kW/m^3, about a factor 30 higher compared to standard dc-glow discharges in TEXTOR-94. Eight chords of the HCN interferometer of sector 14/15 (toroidally 90° away from both antennas) revealed line averaged densities of $1 \times 10^{11} \leqslant n_e$ [cm^{-3}] $\leqslant 3 \times 10^{11}$ across the poloidal cross section as shown in Fig. 3. The density at the outer chord, (low field side) in front of the antennas, was almost a factor 1.5 higher compared to the other. The plasma density increased from the beginning of the process to the end by nearly 1×10^{11} cm^{-3}, measured on all HCN chords.

Table 1
Process parameter of ion cyclotron coating in TEXTOR-94

ICC	
General parameter	
Deposition time (min)	120
First wall temperature (K)	440–460
Wall sample temperatures (K)	300–390
Gas data	
Number of gas inlets	4
Gas mixture	~44% He
	~56% TMB
Gas flow (cm^3/min)	
F_{He}	~15
F_{TMB}	~20
Total pressure (Pa)	4×10^{-2}
TEXTOR-94	
B_t ($r_a = 0$)	0.21 T
Operation mode	steady state
Plasma volume (m^3)	10.5
Pump speed $S_{eff,\,He}$ (l/s)	~1000
Leak rate (mbar l/s)	8×10^{-5}
ICRF-data	
Number of antennae	2 double loop
Antenna A1, sector 10/11	with FS[1)] shielded
Antenna A2, sector 2/3	without FS[1)] unshielded
Coupling efficiency	A1, 80%/A2, 90%
Operation mode	pulsed mode
Duty cycle: plasma on/off (ms)	200/3600

3.2. Analysis of the deposited layers

The samples from both exposure positions (set I in sector 10/11 bottom, set II in sector 5/6 midplane) showed after the removal the characteristic interference colors originated from the deposited layers, which is partly transparent for the visible light. The most important data of the layers obtained by different analysis methods are summarized in Table 2. Interference fringe analysis revealed, that the stainless steel plate of set I was homogeneous covered with a layer of about 50 ± 10 nm. The thickness was confirmed by ellipsometry which also gave the optical constants (refraction index of $n = 1.97$ and absorption coefficient of $k = 0.08$). The layer was abrasive resistant on all materials of sample set I. (In contradiction on set II blistering was observed on stainless steel, Inconel 625 and graphite, while the layer was stable on aluminum and silicon.)

The deposition on the aluminum plate at bottom of set II could not be determined by color fringe analysis since it was below the sensitivity of the method, which is

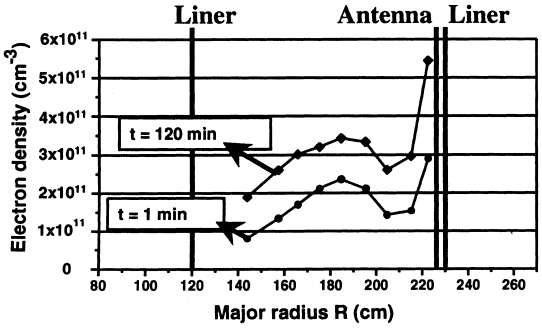

Fig. 3. Line averaged density $\bar{n}_e$ vs. the major radius at the beginning of the process and at the end. The power was constant.

Table 2
Layer properties of wall samples exposed to ICC in TEXTOR-94

Wall samples			
Sample Set	Set 1	Set II	
Position		Bottom	Top
Optical constants			
Refraction (n)	1.97		
Absorption (k)	0.08		
Thickness (nm)	50 ± 10	<20	750 ± 30
Areal mass density (10^{16} atoms/cm^2)			
Boron	3.2		39
Carbon	21		190
Deuterium			170
Oxygen	4.6		76
Atomic ratio			
B/(C + B)	0.13		0.17
D/(C + B)			0.74
Density (g/cm^3)	1.2		1.2
Deposition rate (nm/min)	8	<0.2	120

about 20 nm. For this the surface was not examined by other methods.

The color mapping, of the aluminum plate on top of set II is shown in Fig. 2. One can clearly distinguish three areas. The right-hand side (point A) shows almost no layer. It is the area which was shadowed by the liner and could thus not be reached by the rf-plasma during the deposition process. The area on the left-hand side (point B) was fully exposed to the plasma. There the layer appeared gray and was too thick to be determined by interference fringe analysis. The area in-between, right at the position of the liner appeared colorful and could be quantitatively analyzed until the layer thickness reached 400 nm. The analysis is plotted in Fig. 4 as a function of the distance along the line AB. The filled squares at distances between 26 and 38 cm correspond to the colors originating from the different orders of interference. They correspond to the right Y-axis. Quantitative determination of the areal mass density of boron and carbon was made also along the line AB by means of EPMA. The results are plotted as line scans in Fig. 5. In addition, two silicon samples positioned at distances around 48 and 68 mm next to the line AB were analyzed by EPMA with respect to boron, carbon and oxygen content. They are plotted in the same plot as vertical bars. In order to evaluate the density of the layer, a relation between thickness and areal mass density is needed which was obtained by the overlap of the sum of the areal density of B and C from Fig. 5 on top of the layer thickness curve in Fig. 4. A density of 1.2 g/cm^3 was deduced. To confirm this result furthermore and to measure in addition the deuterium content of the layer, NRA analysis was applied along the same line scan AB and on the Si sample at 48 mm. The result is shown in Fig. 6. The B and C contents obtained by NRA are in good agreement with the EPMA measurement. The areal density of deuterium is listed in Table 2 and the ratio of D/(C + B) was about 0.74. Depth profile measurement of the layers from samples of set I and the set II (top) by sputter AES are in good agreement and show that the boron and carbon concentrations as quantified by EPMA and NRA are constant with the depth. All the data are listed in Table 2 for easy comparison. An un-

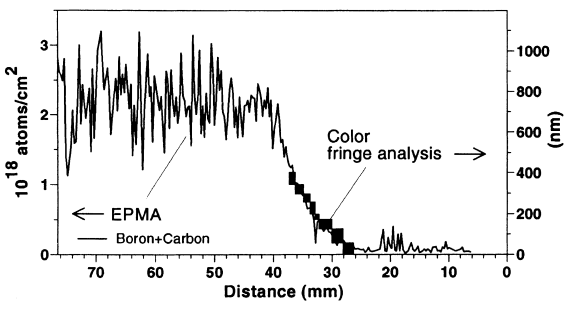

Fig. 4. Thickness determined by color fringe analysis and areal mass density of B + C atoms measured by EPMA on wall sample set II top along line AB.

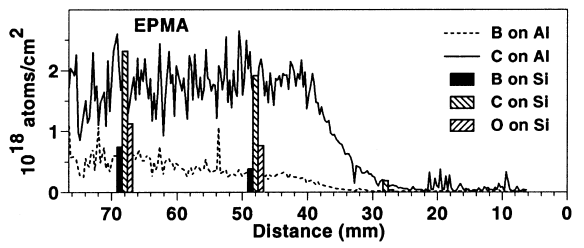

Fig. 5. Areal mass density of B, C, and O measured by EPMA along line AB and on 3 Si-substrates.

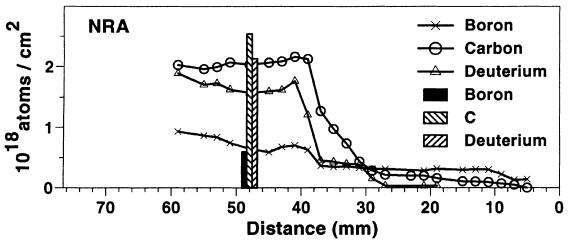

Fig. 6. Areal mass density of D, B, and C measured by NRA along line AB and on a Si-subset.

usual high amount of oxygen was found in the layers. However from the present data, we can not decide about the origin, since a pick up from air after the experiment can not be ruled out.

The data in Table 2 show at first that the deposition process was inhomogeneous on a large scale. A thickness of 50 nm layer at the bottom of sector 10/11 and of 750 nm at the midplane top plate in sector 5/6 has been found. A possible explanation might be that the poloidal position of the samples of set II is just in front of the antennas where the electron densities show more peaking (Fig. 3). Nevertheless the deposition rate of the 50 nm thick layer is already at least a factor 30 higher compared to dc-glow such that the absolute thickness after 6.3 min of plasma time (2000 pulses) is of the order of the thickness of a standard boronization in TEXTOR-94. In addition a strong top to bottom asymmetry of the deposition rate was found at the position of the sample set II. While at the bottom plate nearly no layer was deposited showed the top plate a deposition rate of about 120 nm/min plasma time. This is a rather high value, about 500 times the deposition of a standard dc-plasma boronization in TEXTOR-94. The strong asymmetry may be caused by the separation of charged particles in the toroidal magnetic field due to $E \times B$ forces. This will be proven by reversal of the magnetic field in a coming experiment. The properties of the layers were in general not much different from amorphous layers produced by dc-glow. The somewhat lower density of the films 1.2 g/cm^3 instead of 1.5 g/cm^3 observed in dc-plasma depositions and the higher hydrogen content (0.7 instead 0.3–0.4) at these temperatures, indicate, however, that the films tend more in the direction of soft like films. This might also explain the possible oxygen uptake. Further work will be dedicated to evaluate the influence of the process parameter (pressure, power density, wall temperature etc.) on the film properties.

4. Summary and conclusions

Ion cyclotron coating (ICC) has been successfully tested in TEXTOR-94. The experiment revealed that it is a possible technique to coat inner surfaces of future fusion devices by oxygen gettering materials like boron or silicon. It may replace the standard dc-glow discharge, presently used for boronizations and siliconizations. Experiments at TEXTOR-94 with TMB showed, that it can work reliably in a broad parameter range of magnetic field and gas mixtures containing reactive gases.

The deposition rate varies in a broad range with a value of 120 nm/min at maximum (about 500 times more than in dc-plasma layer deposition) and almost zero. The investigation of the homogeneity of the deposition process needs further measure and has to be studied in more detail.

The properties of the deposited a-C/B:D layer as analyzed ex situ by different surface analyses methods are in general similar to the layers deposited by dc-glow. However, the layer produced in this experiment tends more in the direction of soft layers with lower density and higher hydrogen content. This is probably caused by the energy distribution of the impinging ions on the surface which is probably different compared to dc-glow discharges. The process parameter like pressure, plasma density, gas mixture and power density, wall temperature etc. have to be optimized and can be varied in a broad range. One further advantage of the method is, that probably most of new future devices will be equipped with ICRF-systems for plasma heating in any case.

Acknowledgements

The authors would like to thank Dr H.R. Koslowski for providing data concerning electron density measurements.

References

[1] U. Samm, P. Bogen, H.G. Esser et al., J. Nucl. Mater. 220–222 (1995) 25.
[2] J. Winter, in: W. Hofer, J. Roth (Eds.), Physical Processes of the Interaction of Fusion Plasmas with Solids, vol. 6, p. 217–241.
[3] H.G. Esser, A.I. Lyssoivan, M. Freisinger et al., J. Nucl. Mater. 241–243 (1997) 861.
[4] E. Gauthier, E.E. de la Cal, B. Beaumont et al., J. Nucl. Mater. 241–243 (1997) 553.
[5] A.I. Lyssoivan, O. Neubauer, R. Koch et al., Proceedings of 24th EPS Conference on Controlled Fusion and Plasma Physics, Berchtesgaden, vol. 21A, Part IV, 1997, p. 1741.
[6] E. de la Cal, E. Gauthier et al., Plasma Phys. Contr. Fusion 39 (1997) 1083.
[7] J. Winter, J. Nucl. Mater. 145–147 (1987) 131.
[8] J. Winter, H.G. Esser, L. Könen et al., J. Nucl. Mater. 162–164 (1989) 713.

[9] J. Winter, H.G. Esser, G.L. Jackson et al., Phys. Rev. Lett. 10 (1993) 1549.
[10] H.G. Esser, H. Reimer, J. Winter et al., Fusion Technol. 1 (1988) 791.
[11] J. Winter, H.G. Esser, H. Reimer et al., J. Nucl. Mater. 176&177 (1990) 486.
[12] H.G. Esser, J. Winter, V. Philipps et al., J. Nucl. Mater. 212–215 (1994) 1546.
[13] R. Van Nieuwenhoven et al., Nucl. Fusion 32 (1992) 1913.
[14] A.I. Lyssoivan et al., Nucl. Fusion 32 (1992) 1361.
[15] A.I. Lyssoivan et al., Proceedings of Second Europhysics Topical Conference on RF Heating and Current Drive of Fusion Devices, Brussels 1998, vol. 22A, p. 85.